EFFECT OF STRUCTURAL VARIABILITY OF THE CERAMIDE PART ON THE SACCHARIDE-CERAMIDE LINKAGE IN MODEL GLYCOLIPIDS STUDIED BY MOLECULAR MECHANICS AND MOLECULAR DYNAMICS METHODS

Zuzana GALOVA[1] and Tibor KOZAR[2,*]

Department of Biophysics,Institute of Experimental Physics, Slovak Academy of Sciences, Watsonova 47, 043 53 Kosice, Slovak Republic; e-mail: [1] galova@linux1.saske.sk, [2] tibor@gd.glycodesign.com

Received May 5, 1995
Accepted November 6, 1995

Conformational analysis was performed for model glycosphingolipid molecules with a view to studying the effect of structural variability of the lipidic part and its flexibility on the saccharide-ceramide linkage. In addition to systematic and random molecular mechanics sampling techniques (the RAMM program), molecular dynamics simulations (Biosym DISCOVER program) were carried out to analyze the conformational energy surface of the model glycolipid molecules. The influence of the structural variability and flexibility of the lipidic part is demonstrated by prediction of the stability of different conformations around the carbohydrate-ceramide linkage. The α_2, α_1 and Θ_1 torsional angles are the most important structural parameters with respect to the carbohydrate-ceramide connection. Two dominant conformations for the saccharide-ceramide linkage were observed, with the $\alpha_2/\alpha_1/\Theta_1$ dihedral angles in the *–sc/+ac/ap* and *–sc/ap/–sc* regions. While each of the calculation methods predicts similar flexibility in the α_2/α_1 space, the flexibility around the Θ_1 angle differs considerably, reflecting the parametrization and set-up of the modelling protocol.

Key words: Glycosphingolipids; Monoglycosyl-ceramide; β-Glycosidic linkage; Molecular mechanics; Molecular dynamics; Conformational analysis.

Glycolipids (GLs), in particular glycosphingolipids (GSLs), are structurally heterogeneous groups of membrane components that are found in biological species ranging from bacteria to the human organism. GSLs consists of mono- or oligosaccharides whose reducing end is glycosidic-linked to ceramide. GSL molecules perform various biological functions in membranes[1,2] and are of interest with respect to their role as receptors for bacteria and viruses[3]. The structural heterogeneity of GSLs includes a structural diversity of both the saccharide and ceramide parts of the molecules. Recent studies on GSLs suggest that not only the structure and orientation of the saccharide

* Present address: Glycodesign Inc., 480 University Avenue, Suite 900, Toronto, Ontario, Canada M5G 1V2

chain at the membrane surface but also the structural variability of the ceramide part (i.e. unsaturation of the sphingosine chain and hydroxylation of the fatty acid chain) is important for the recognition of GSLs by antibodies and bacterial adhesines, for the binding activity and membrane stability[1,4,5]. As yet, the role which the structural variability in the ceramide part of GSLs plays with respect to the orientation of the saccharide head group relative to the bilayer has not been recognized. One of the reasons is the difficulty in the preparation of appropriate amounts of pure and well-defined GSLs-species for experimental studies.

For few monoglycosyl-sphingolipids molecules[4,6,7] was the three-dimensional structure determined by diffraction studies. NMR conformational studies are also rare in the literature[8]. Moreover, the saccharide head group can take two orientations – parallel or perpendicular – relative to the layer (cell) surface. This is why computer experiments, directed to static or dynamic modelling of the conformational behaviour of glycolipids, can contribute substantially to our understanding of the driving forces that determine the stability of the molecular conformations.

Conformational analysis of β-D-glucosyl-*N*-(2-D-hydroxyoctadecanoyl)-D-dihydrosphingosine (β-glucosyl-ceramide) was introduced by Wynn, Marsden and Robson[9] almost a decade ago. Using empirical energy functions and the simplex method for geometry optimisation, the authors were able to show that the lowest-energy conformation of the β-glucosyl-ceramide assumes a parallel orientation of the monosaccharide moiety to the membrane bilayer. These findings were supported by X-ray structure studies of β-galactosyl-ceramide[7]. Wynn et al.[9] used the simple 6-9 potential energy function to describe non-bonding interactions and point-charge approximation for the electrostatic term. In recent conformational studies, Nyholm et al.[4,10,11] applied the well-established molecular mechanics method of Allinger (versions MM2-87 (ref.[12]) and MM3 (ref.[13])) to analyze native and methylated monoglycosyl-ceramides. In MM2/MM3 the electrostatic energy contribution is described by bond dipoles. Concurrently, the semiempirical quantum chemical AM1 method (using the MOPAC program) was also introduced to calculate the energies of selected conformations of β-glucosyl-ceramide[10].

As has been shown for the native cerebroside[4], the hydrogen bonding between the amide N–H group and the glycosidic oxygen is responsible for the orientation of the monosaccharide head-group. If this hydrogen bond is present, the monosaccharide orients parallel to the layer. If the hydrogen bond is absent, e.g. in the case of the permethylated structure, the monosaccharide is oriented perpendicular to the bilayer. The Θ_1 torsional angle (see Fig. 1) plays an essential role in the description of the orientation of the GSL structures relative to the membrane surface. Nyholm et al.[4] have shown that the amide-glycosidic oxygen intramolecular hydrogen bond occurs in the *–sc* orientation of the Θ_1 angle around the C1–C2 bond ($\Theta_1 = -75°$). The *+sc* ($\Theta_1 = 69°$) and *ap* ($\Theta_1 = -175°$) minima were found 2.2 and 2.0 kcal/mol less stable as the global

–sc minimum. A comparison of 11 crystallographic data of relevant glycolipids (glycerolipids also considered) showed[4] that the *+sc* : *ap* : *–sc* ratio of the Θ_1 angle is 1 : 8 : 8. Thus the prediction of preference of the *–sc* orientation, as emerged from the MM2 calculation, seems to be reasonable.

All of the calculations discussed were static in their nature and did not take into account the time dependence of the conformational changes in the glycolipid molecules. The necessity of including dynamic features into theoretical studies on membrane components is beyond doubt. Molecular dynamics simulations are capable of modelling the motions of molecules. They are increasingly applied to explore the conformational space of carbohydrates[14]. Similarly, molecular dynamics simulations have been applied with success to the investigation of phospholipids[15–20]. To our knowledge, molecules of monoglycosyl-ceramides have not yet been studied by this tool. The primary aim of the presented study was to bridge the gap between the static and dynamic conformational search protocols for this type of glycoconjugates. This work shall also

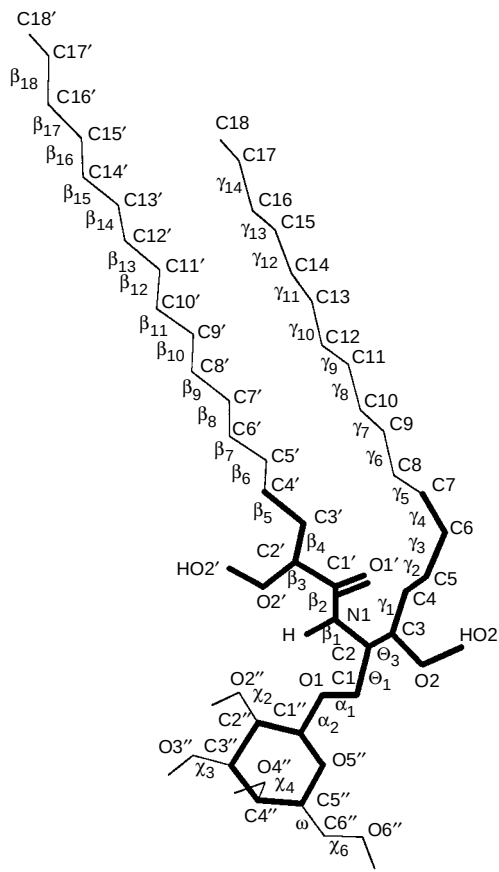

FIG. 1
Monogalactosyl-ceramide; atom numbering according to Sundaralingham[27]. The torsional angles are designated as follows: α_2 = O5"–C1"–O1–C1; α_1 = C1"–O1–C1–C2, Θ_1 = O1–C1–C2–C3; Θ_3 = C1–C2–C3–C4; γ_1 = C2–C3–C4–C5; γ_2 = C3–C4–C5–C6; β_1 = C1–C2–N1–C1′; β_2 = C2–N1–C1′–C2′; β_3 = N1–C1′–C2′–C3′;… The glycolipid model molecule used in the presented study is indicated in bold

contribute to a better understanding of the relationship between the structural variability of the ceramide part and the preferred conformational regions of the carbohydrate-ceramide linkage.

COMPUTATIONAL METHODS

Molecular Mechanics

GSLs are highly flexible molecules. As indicated with Greek letters in Fig. 1, there are over 40 rotatable bonds in a monogalactosyl-ceramide molecule around which conformational changes can take place. Regular-grid conformational search considering all of the rotational degrees of freedom is not practical even on the platform of state-of-the-art workstations. An alternative approach has been proposed, referred to as the **RA**ndom, **M**olecular **M**echanics[21] (RAMM) protocol, which optionally combines three independent calculation methods: (*1*) random sampling of the *n*-dimensional conformational energy surface, (*2*) regular-grid conformational search for selected torsional angles, and (*3*) minimization of molecular energy. Combinations of all of these options have been used in the present study: (i) regular scanning of the conformational energy surface for selected pairs of torsional angles (two-dimensional sections from the *n*-dimensional surface), (ii) random generation of ensembles with different torsional angles, (iii) simultaneous optimization of the torsional angles of low-energy conformers from randomly generated ensembles, and (iv) consequent global optimization of all degrees of freedom, i.e. all internal coordinates (torsional and bond angles and bond lengths) for both the regular-grid and random-generated geometries. The energy calculation for all steps (i) through (iv) follows the well-established MM2-87 force field of Allinger[12]. Bond dipoles were used in the electrostatic energy contribution. Lone pairs were included for all heteroatoms. No special function was added to account for hydrogen bonding, which in the MM2 series is directly included in the force-field parametrization.

Due to the complexity of the potential energy surface of the molecules under study, the fact that two differently generated geometries can converge to one point on the energy surface after geometry optimization is a source of perplexity of the random sampling method. This problem becomes more serious with increasing complexity of the potential energy surface of the molecule studied. Therefore, identical conformers were eliminated from the final set of minimized conformers of the GSLs. Geometry and energy criteria were applied to this. The identity of the conformers was tested by calculating the *rms* deviation of their cartesian coordinates, and the conformers with identical *rms* deviations were discarded from the set. Where a low *rms* difference between two conformers was obtained, their energy values were used to judge the identity of the two conformations. The *rms* values were also used to divide the conformers into

families (clusters). The population distribution x_i for the different conformers was calculated assuming the Boltzmann distribution at 298 K.

Two independent sets of calculations were carried out. In the first, the standard MM2 value of the dielectric constant ($\varepsilon = 1.5$) was applied. In the second, a dielectric constant of 4 was used, a value appropriate for carbohydrates, in accordance with the proposal of French and Dowd[22]. The value of the dielectric constant for glucosyl-ceramide conformational analysis, performed by the MM3 method, has been tested recently ($\varepsilon = 1.5$; 4 and 80) by Nyholm et al.[10,11]. The dielectric constant $\varepsilon = 4$ has also been shown[10] to be consistent with the experimental observations[23] (ε between 4 to 10) for the head-group region of phospholipids; corresponding experimental data for glycolipids are unavailable so far.

Molecular Dynamics (MD)

The DISCOVER program (Versions 2.95) of Biosym Technologies of San Diego, running on a Silicon Graphics workstation, was used for molecular dynamics simulations. No carbohydrate or lipid-specific alteration was applied to the standard **C**onsistent **V**alence **F**orce **F**ield[24–26] (CVFF). Equation (*1*) illustrates the analytic forms of the energy terms used optionally in CVFF:

$$E_{\text{pot}} = \sum_b D_b(b - b_0)^2 + \sum_\Theta H_\Theta(\Theta - \Theta_0)^2 + \sum_\Phi H_\Phi[1 + s\cos(n\Phi)] +$$

$$+ \sum_\chi H_\chi\chi^2 + \sum_b \sum_{b'} F_{bb'}(b - b_0)(b' - b'_0) + \sum_\Theta \sum_{\Theta'} F_{\Theta\Theta'}(\Theta - \Theta_0)(\Theta' - \Theta'_0) +$$

$$+ \sum_b \sum_\Theta F_{b\Theta}(b - b_0)(\Theta - \Theta_0) + \sum_\Phi F_{\Phi\Theta\Theta'}\cos\Phi(\Theta - \Theta_0)(\Theta' - \Theta'_0) +$$

$$\sum_\chi \sum_{\chi'} F_{\chi\chi'}\chi\chi' + \sum \varepsilon[(r^*/r)^{12} - 2(r^*/r)^6] + \sum q_i q_j/\varepsilon r_{ij} \quad . \qquad (1)$$

The first four terms in Eq. (*1*) represent the energy of distortion of the bond lengths (b), bond angles (Θ), torsional term (Φ) and out-of-plane interactions with the corresponding force constants D and H. The next five contributions are off-diagonal or cross-terms. The last two terms in Eq. (*1*) correspond to the non-bonding (Lennard–Jones function) and electrostatic contributions with point-charges (q_i and q_j). In addition to the molecular dynamics simulation considering all terms in Eq. (*1*), simulations with a

simplified potential energy function, i.e. omitting all cross-terms from Eq. (*1*), are also presented for the model glycolipid molecules.

The Verlet algorithm was used for the integration of Newton's equations of motion with the leapfrog version. No CUTOFFs or SHAKE approximation was applied during the calculations in the all-atom approach. In contrast to the MM2 method described above, heteroatom lone pairs are not required within the frame of the CVFF. The atomic point-charges, necessary for the electrostatic contribution (Eq. (*1*)), were established using the automatic assignment procedure of the BUILDER module in the INSIGHTII program of Biosym Technologies, in accordance with the pre-set CVFF parametrization. Several molecular dynamics simulation protocols (up to 1 000 ps) were carried out at 300 K with a 1 fs integration step. The thermodynamic parameters, the atomic velocities and coordinates during the simulation period were saved for further processing at time intervals of 0.25 ps. The ANALYSIS module of the INSIGHTII was used to examine the trajectories. For the analysis, an 1 ps interval was set to read in trajectory data. The time dependences of the simulation temperature and the total energy of the molecule, composed of the potential and kinetic energies, were selected as the main parameters to assess the stability of the simulation. After the equilibration period (20 ps for each molecule), only small fluctuations around the equilibrium values were observed and no intervention was thus necessary to maintain the simulation temperature.

The lowest-energy conformers from the RAMM modelling were used as the starting geometries for the molecular dynamics simulation. At the beginning of the simulation, all geometries were re-optimized to achieve low gradients in the CVFF force field. As in the RAMM modelling, two sets of molecular dynamics simulations with dielectric constant values of $\varepsilon = 1$ and $\varepsilon = 4$ were carried out.

The DISANA program was used for the trajectory analysis and for calculation of the counts of occurrence of the given torsional angle within a certain conformational region. The time-averaged values and standard deviations of the geometric parameters were also calculated by DISANA.

Model

The scheme of β-galactosyl-ceramide is shown in Fig. 1 (the atom numbering and conformational variables, i.e. torsional angles, are defined in accordance with Sundaralingam[27]). Since the number of rotatable torsional angles is high (exceeding 40), the multiple-minimum problem[28] is encountered in the glycolipid molecule. As a consequence, a systematic conformational sampling of all degrees of freedom is difficult on the molecular mechanics level. Li and Scheraga[29] have shown for the Monte Carlo algorithm that the efficiency of sampling of the conformational space of biomolecules can be increased if the number of the variables (torsional angles) is reduced. In the case of the glycolipid molecules, where the conformational behaviour of the saccharide-ceramide linkage is of particular interest, several simplifications can be made to increase

the efficiency of the molecular mechanics sampling protocol and thus to save computer time. First, assuming a high probability of the all-trans orientation of the –C–C–C–C– torsional angles in the hydrocarbon chains of the lipidic part, the chains can be shortened to a few atoms. Second, it is convenient to replace the monosaccharide moiety by an unsubstituted pyranose ring, that is, to substitute the glucose or galactose residues present in native, natural monoglycosyl-ceramides with a tetrahydropyran (THP) molecule having no primary or secondary hydroxy groups. In addition to saving computation time, the asset of such a model is that it represents both galacto- and gluco-ceramides; the drawback of the model is that the occurrence of the lateral intramolecular hydrogen bonding between the pendant groups of the monosaccharide and the lipidic part is explicitly excluded. Still, the model is physically meaningful because it represents the optional hydrogen bonding between the glycosidic or ring oxygens of the model head group and the amide or oxygen atoms of the lipidic part.

Four model molecules were set up to study the effect of the ceramide substitution on the saccharide-ceramide linkage: with or without a hydroxyl group in the fatty acid chain, and with or without a double bond between the C4 and C5 atoms in the sphingosine chain. The models are designated as follows: **HD** a glycolipid with both a hydroxy group in the fatty acid chain and the C4=C5 double bond present in the sphingosine chain of the molecule; **HS** a glycolipid having a hydroxy group in the fatty acid chain and with no multiple bonds in the hydrocarbon chain; **ND** a glycolipid without any hydroxy group in fatty acid and with the C4=C5 double bond in the sphingosine chain; and, finally, **NS** the unhydroxylated model molecule with all C–C bonds saturated.

The conformational energy profiles, calculated for all above models, are presented as two-dimensional energy maps for selected pairs of torsional angles, mainly α_1, α_2 and Θ_1. The conformational space for the other torsional angles, in the case of the molecular mechanics conformational search, was sampled in a random manner and the geometry of the low-energy conformations was also optimized. For the molecular dynamics calculation the resulting trajectories of the torsional angles are represented as time dependences of the angles, or as two-dimensional plots, showing the distribution of the torsional angles in the α_2, α_1 and α_1, Θ_1 space.

In both sampling protocols – random molecular mechanics and molecular dynamics – only the properties of the isolated glycolipid molecule were modelled, without explicit inclusion of molecules of the biological environment (proteins, membranes, water of counter ions). Because modelling of the conformational properties of the saccharide-lipid linkage was the main goal of the present study aimed specially at ascertaining the existence of hydrogen bonding between the amide N–H and oxygen of the pyranose ring or glycosidic linkage, we consider the approximation of the isolated molecule appropriate.

RESULTS AND DISCUSSION

Conformational Flexibility

Four sets of molecular dynamics simulations were carried out for the four molecules under study: with and without the cross-energy terms (see Eq. (*1*)), both with dielectric constants of 1 and 4. As selected examples of results of the 16 simulations, Figs 2–5 illustrate the summaries of the molecular dynamics trajectories (i.e. time dependences) for the four model molecules, considering all cross-energy terms in Eq. (*1*) and the electrostatic part calculated with a dielectric constant of 4. As the energy profiles demonstrate ("Total E" on the right bottom in the figures), all of the simulations were fairly stable. The average temperature and energy values and the standard deviations, as cal-

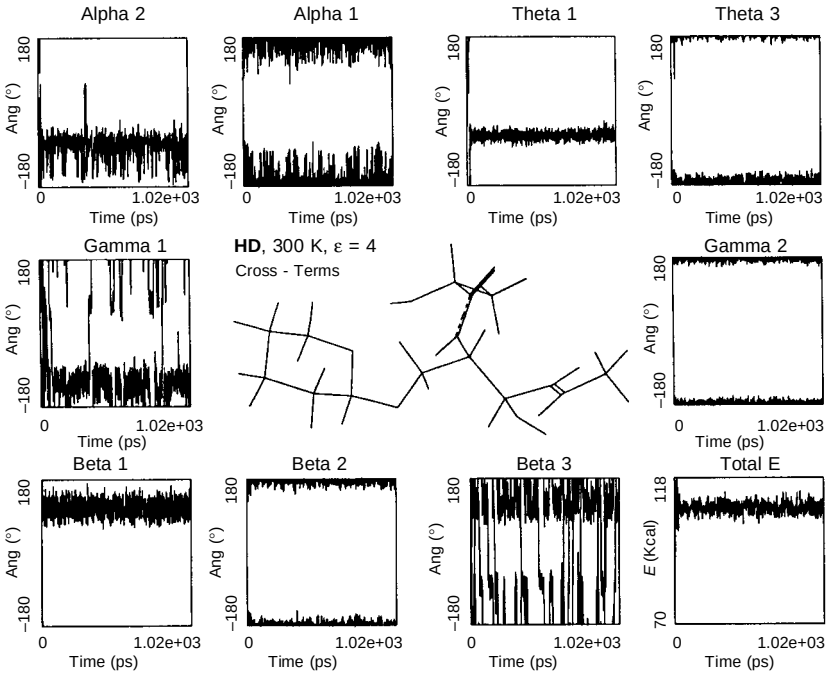

FIG. 2

Time-dependences (trajectories) of selected torsional angles and of the total energy of the **HD** molecule as obtained from a 1.02 ns molecular dynamics simulation, calculated by the DISCOVER program. All cross-energy terms were included in the CVFF force field simulation at T = 300 K with a dielectric constant $\varepsilon = 4$. The starting geometry of the molecule is shown in the middle of the figure. The trajectories of the torsional angles, illustrating the conformational changes of the sugar-ceramide linkage and the mobility of the lipidic chains (α_2, α_1, Θ_1, Θ_3, γ_1, γ_2, β_1, β_2 and β_3 starting in upper-left graph); the trajectory of the total energy of the simulated system is shown in the bottom-right graph

culated by DISCOVER, are summarized in Table I. Similar energy curves (not shown) were also obtained from the simulation with $\varepsilon = 1$ and from the two consequent simplified simulations without explicit inclusion of the cross-energy terms. The small deviations from the mean values further confirm the stability of the simulation. The $^4C_1$ chair conformation of the pyranose ring was stable during all 16 simulations and no chair-skew interconversions were observed. Also the CO–NH bond remained *trans*, with insignificant fluctuations about the time-averaged value (see "Beta 2" in the Figures). The same is valid for the C4=C5 double bond in the **HD** and **ND** molecules (see "Gamma 2" in Figs 2 and 4). On the other hand, where there was a single bond between C4 and C5 (**HS** and **NS** molecules in Figs 3 and 5), several excursions from the dominant *ap* to ±*sc* orientations occurred with a longer life-time on the time-scale for the **HS** molecule. The changes in the β_1 and the β_3 torsional angles ("Beta 1" and "Beta 3" in the figures) are similar for the molecules studied, but with fewer transitions from the dominating +*sc* region for **HS** and **HD** than for **NS** and **ND**.

The conformational flexibility around the α_2 and α_1 torsional angles is also similar for all of the molecules studied. This was confirmed with both modelling protocols, molecular mechanics (see the two-dimensional conformational energy plots for these

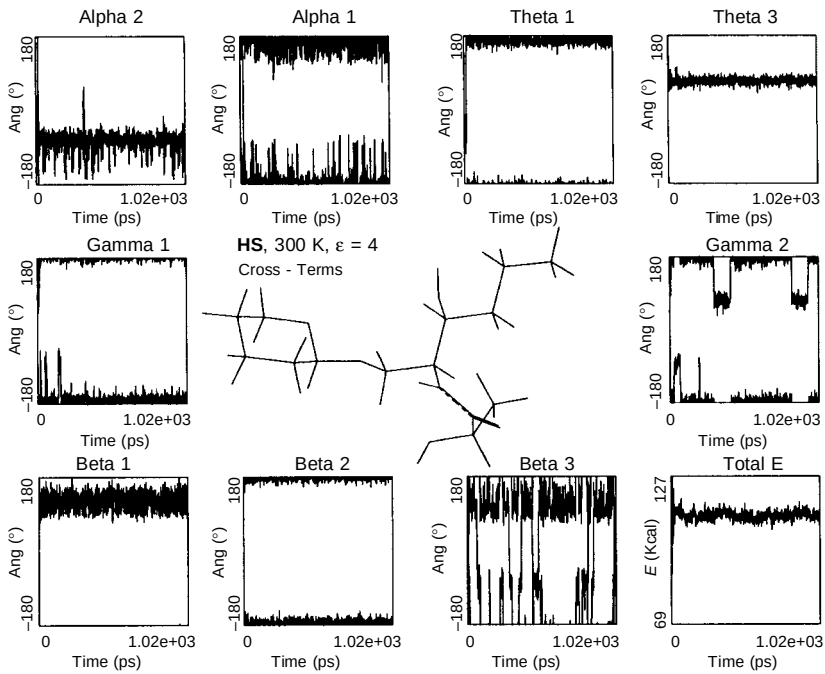

FIG. 3
Trajectories of the **HS** molecule. Description as in Fig. 2

angles, calculated with RAMM and shown in Fig. 6) and molecular dynamics (see the two-dimensional representation of the 1.02 ns trajectories as α_2 and α_1 scattering in Fig. 7). Both figures were obtained at low dielectric constants (1.5 for RAMM and 1 for CVFF). Increasing the dielectric constant to 4 has no appreciable effect on the shape of the energy curves or on the scatter of the α_2 and α_1 angles analyzed. In accordance with the consequences of the *exo*-anomeric effect for the equatorial glycosidic bond, the *–sc* region of the α_2 angle defines the dominant conformation but the molecules also probe the conformational regions directed toward the *+sc* orientation of the given angle. For all the molecules studied, the main conformational region for α_1 is between the *+ac* and *ap* regions and the fluctuations from this region vary only slightly from molecule to molecule.

The agreement of the calculated conformational preference for the α_2 angle (*–sc* orientation for all molecules under study) with the crystallographic data of native (–79° and –84° for the two molecules in a unit cell of CER, ref.[7]) and methylated galactosylceramide (–69° in MCER, ref.[4]) is good. It should be pointed out that no special energy terms were used in the RAMM calculations to account for the *exo*-anomeric effect. The second conformational region for α_2 is located in the *+sc* region. The population of this

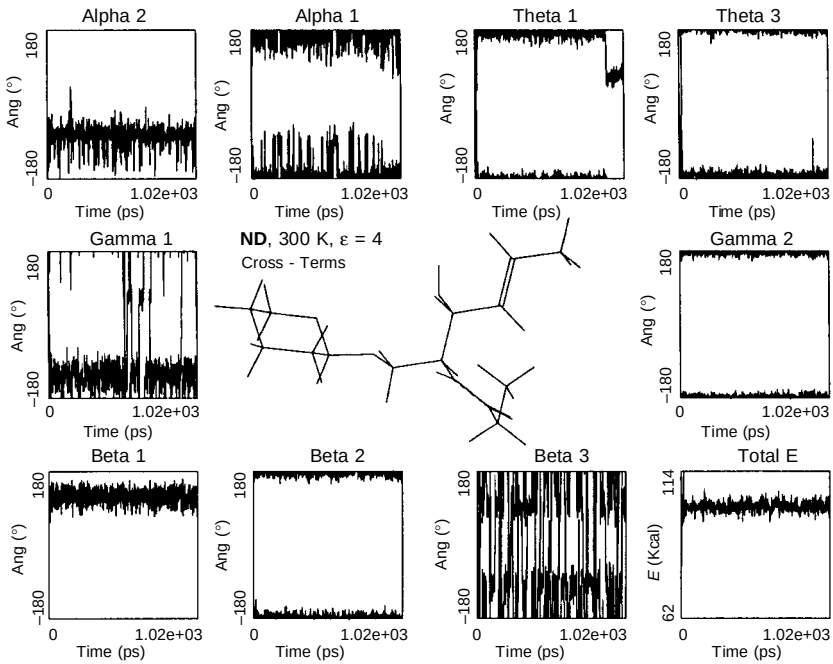

FIG. 4
Trajectories of the **ND** molecule. Description as in Fig. 2

region is below 5.2% (Table II). Whereas there is no experimental evidence for the occupancy of the +*sc* region of α_2 for glycosyl-ceramides, this conformer was observed several times for phospholipids, as demonstrated, for example, by the crystallographic data of GPC, 64° (ref.[30]), LPPC, 86° (ref.[31]), PE, 51° (ref.[31]), DLPE, 58° (ref.[32]) and DMPC, 68° (ref.[33]). Neither the differences in the chemical composition of the ceramide part nor the value of the dielectric constant used in calculation affected the preference of the dominating –*sc* conformational region of α_2.

Table III summarizes in detail the results of flexibility of the α_2, α_1, Θ_1 torsional angles from all MD simulations as calculated by the DISANA program. The time-averaged values from the entire simulation are indicated in bold. The mean values within the occupied conformational regions of the α_2, α_1, Θ_1 torsional angles are given for all the 16 molecular dynamics simulations. If the mean value of the torsional angle, characterizing the dominant conformational region, approaches the time-averaged value from the whole simulation, low flexibility with one dominant conformation is assumed. Several examples are given in Table III.

The main difference in the conformational freedom of the molecules under study appears in the flexibility of the Θ_1 torsional angles. Transitions between the different

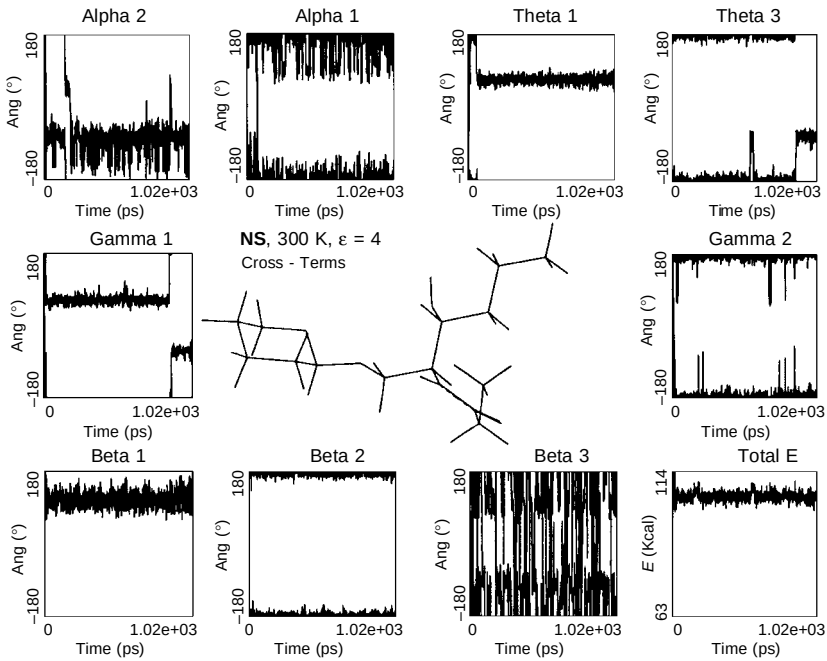

FIG. 5
Trajectories of the **NS** molecule. Description as in Fig. 2

conformational regions of the Θ_3 and γ_1 angles are also predicted by the MD simulations (see Figs 2–5 for illustration). But because the direct influence of these angles on the ceramide-sugar orientation is presumably of lower importance than that of the Θ_1 angle, we will not discuss the conformational changes around the Θ_3 and γ_1 angles in detail.

There are three low energy conformational regions for the Θ_1 angle: +*sc* located around 60°, *ap* around 180°, and –*sc* around –60°. The localization of these regions is evident from the RAMM modelling and is illustrated in Fig. 8 where the two-dimensional α_1/Θ_1 conformational energy plots are presented. The conformational energy profiles shown were calculated with a dielectric constant of 4. The influence of the

TABLE I

Averaged energy and temperature values and standard deviations (SD) of glycolipid molecules. CVFF parametrization in 1.02 ns DISCOVER molecular dynamics simulation at 300 K with all cross-energy terms included and dielectric constant ε = 4. The energies are in kcal/mol (1 kcal/mol = 4.1868 kJ/mol), the temperature in K

Molecule	Parameter	20 ps equilibration		1 000 ps simulation	
		average	SD	average	SD
HD	Total energy	106.647	5.892	107.914	1.741
	Potential energy	66.424	5.948	67.641	3.593
	Kinetic energy	40.223	1.123	40.273	3.358
	Temperature	299.868	8.369	300.241	25.034
HS	Total energy	113.047	6.263	111.768	1.742
	Potential energy	71.019	6.329	69.705	3.681
	Kinetic energy	42.028	1.178	42.063	3.467
	Temperature	299.990	8.411	300.239	24.750
ND	Total energy	100.638	5.830	101.759	1.663
	Potential energy	61.298	5.894	62.383	3.546
	Kinetic energy	39.340	1.102	39.376	3.326
	Temperature	299.951	8.399	300.222	25.362
NS	Total energy	106.586	6.372	105.465	1.653
	Potential energy	65.466	6.450	64.299	3.621
	Kinetic energy	41.120	1.216	41.166	3.429
	Temperature	299.891	8.872	300.225	25.007

dielectric constant on the shape of the profiles, as resulted from the RAMM modelling, is only moderate. The main conformational regions are those at *ap*/–*sc*, +*ac*/*ap* for α_1/Θ_1. The population of the third region, located approximately at *ap*/+*sc*, is low due to the higher energy of this minimum.

The MD simulation ($\varepsilon = 1$, no cross-energy terms) indicates that the main conformational region for α_1 is centered around 180° with the following average values: **HD**: 180.0° (57.3%); **HS**: 175.6° (58.8%); **ND**: 175.5° (48.8%); **NS**: 175.4° (58.5%) (the values in

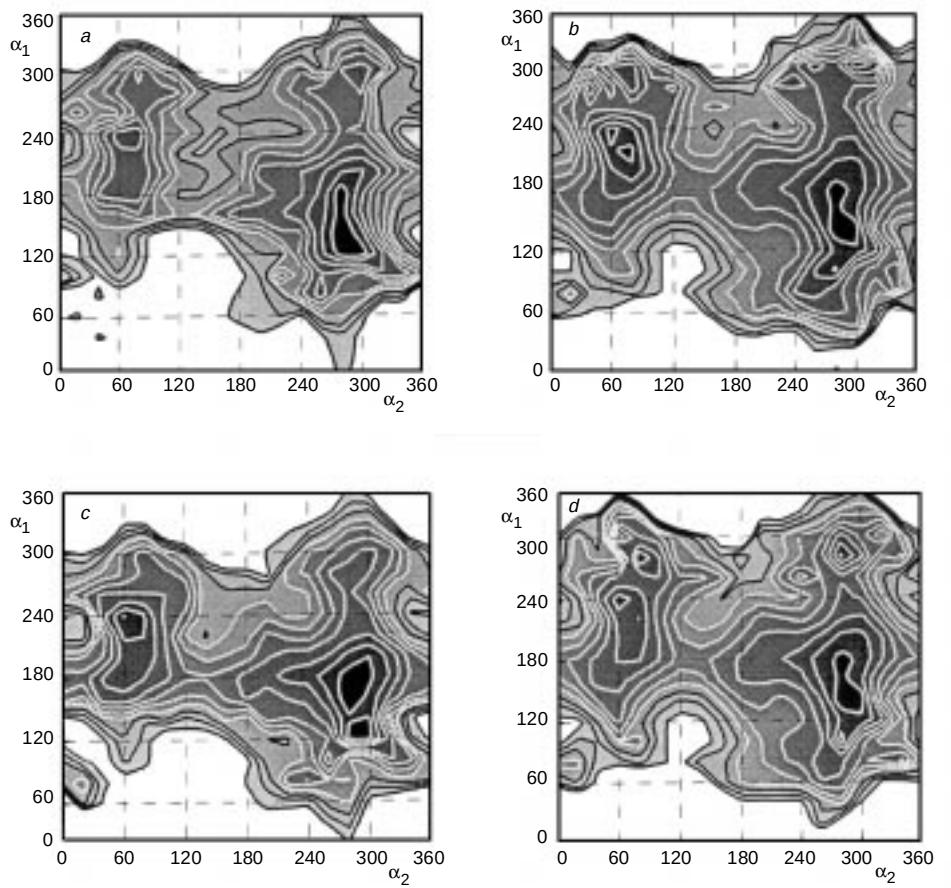

FIG. 6

Conformational energy maps (α_2/α_1), calculated by RAMM ($\varepsilon = 1.5$). Energy levels up to 10 kcal/mol above the global minimum with a 1 kcal/mol interval are shown, the low-energy contours (1–7 kcal/mol) in white and the higher energy contours (9–10 kcal/mol) in black. The colour scale for filling the conformational regions is opposite, i.e. dark for minima and white for regions above 10 kcal/mol. *a* **HD**, *b* **HS**, *c* **ND**, *d* **NS** model molecules

TABLE II
Boltzmann distribution x_i (%) of the –*sc* and +*sc* rotamers of α_2 at 25 °C

Molecule	ε = 1.5		ε = 4.0	
	–*sc*	+*sc*	–*sc*	+*sc*
HD	98.12	1.53	97.18	1.92
HS	99.75	0.19	99.76	0.15
ND	94.64	5.19	98.03	1.42
NS	99.98	0.01	99.92	0.0

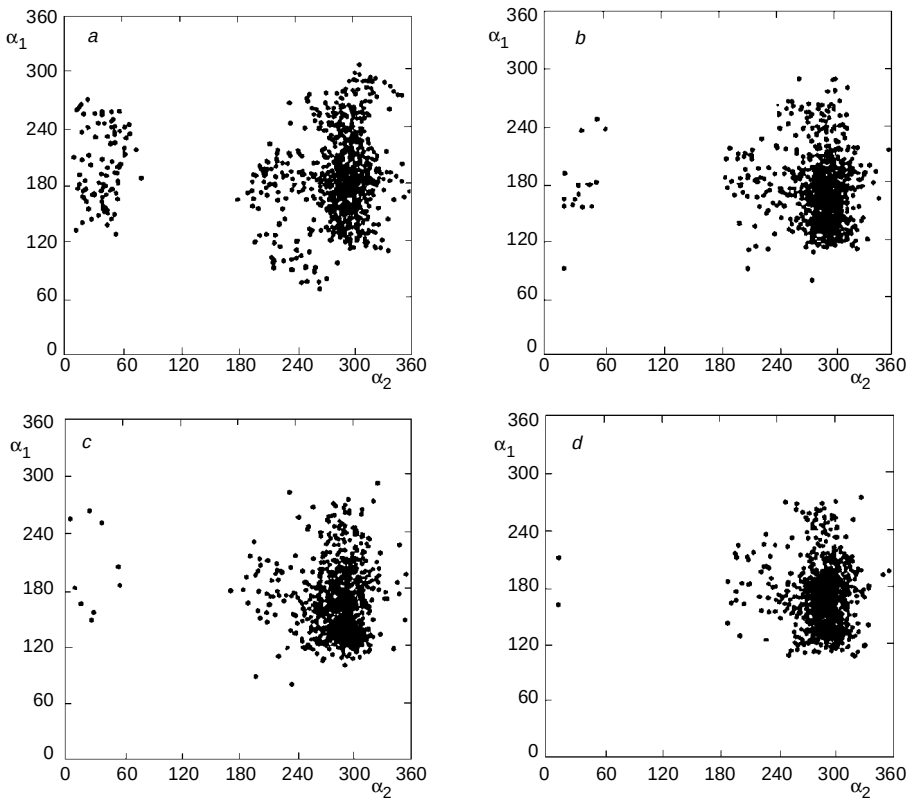

FIG. 7
Fluctuation of the α_2/α_1 torsional angles, as obtained from the 1 020 ps molecular dynamics simulation (asterisks). *a* **HD**, *b* **HS**, *c* **ND**, *d* **NS** model molecules

brackets indicate the time proportion of the 1 020 ps interval during which the α_1 angle oscillates within the given conformational region). In accordance with the MD, additional well-defined minima for α_1 are located in the +*ac* region around 120° and the –*ac* regions around –120° (Table III).

Performing MD simulations with different computational set-ups, we observed significant differences in the flexibility around the Θ_1 dihedral angles. Figure 9 shows the two-dimensional plots of the scattering of the α_1/Θ_1 angles for all prototype molecules as emerged from the 1.02 ns molecular dynamics simulation. In this example (a dielectric constant of 1 was used in the electrostatic part and no cross-energy terms included in the energy expressions), only one preferred conformational region (–*sc*) for the Θ_1 angle was obtained, in contrast to the molecular mechanics calculation. On the other hand, the distribution for α_1 is very similar to the prediction from molecular mechanics and is ranging between +*ac* and *ap* with a certain spread out toward –*ac*.

When all cross-energy terms were included in the calculation, in the case of **HD** and **HS** the preference of the –*sc* region prevailed, whereas in the case of **ND** and **NS** the Θ_1 angle jumped immediately during the equilibration period to the +*sc* domain. The α_1 distribution was not influenced appreciably.

In the molecular dynamics simulation with the same calculation setup (i.e. cross-energy terms included) but with a dielectric constant of 4, the α_1/Θ_1 scattering (not shown) was even more diverse for the Θ_1 angle: –*sc* for **HD**, *ap* for **HS**, *ap* and certain occupancy of +*sc* for **ND**, and +*sc* becoming the main conformational region for **NS**. Diverse results were also obtained for the same angles from the simulation with a dielectric constant of 4 and with no cross-energy terms. Here, the results for the **NS** and **ND** molecules are equivalent to the simulation with the dielectric constant of 1 and with no cross-terms. The α_1/Θ_1 scattering for **HD** is located mainly in the *ap* region for Θ_1.

The most interesting scattering of the α_1/Θ_1 angles was obtained for the **NS** molecule, where all the three possible minima for Θ_1 occur, with the approximately 60 : 32% ratio of occurrence of Θ_1 in the +*sc* and *ap* regions and a lower occupancy of the –*sc* region (Table III). The dielectric constant of 4 was used in this MD simulation and the cross-energy terms were not included. This example shows the best agreement of the conformational behaviour of the Θ_1 angle as emerged from the molecular dynamics simulation with the findings from the RAMM modelling and from the recent conformational study of related molecules[10,11].

Conformational Equilibrium

The α_2, α_1 and Θ_1 torsional angles can be regarded as the most important parameters to characterise the carbohydrate-ceramide connection. In the previous section, two-dimensional conformational energy maps and two-dimensional scattering have been used to obtain essential information for the distribution of these angles. The conformational energy maps can be considered as "superposed adiabatic" profiles, because each grid

TABLE III

Average values (AV), standard deviations (SD) and counts of occurrence (*N*) of the torsional angle within the given conformational region as obtained from 1 ns molecular dynamics simulations. Concurrent counts below 1% for all molecules are not shown. The time-averaged values from the entire simulation (*N* = 1 020) are indicated in bold

Angle/ conformational region	HD			HS			ND			NS		
	AV	SD	*N*	AV	SD	*N*	AV	SD	*N*	AV	SD	*N*
a) calculation without cross-energy terms and ε = 1												
α_2	**–62.5**	**42.4**	**1 020**	**–73.0**	**26.4**	**1 020**	**–73.1**	**26.3**	**1 020**	**–72.5**	**21.2**	**1 020**
sp	3.2	19.7	49	–1.8	21.9	12	–3.1	19.2	14	–14.2	17.1	8
+sc	47.0	10.1	65	42.7	9.9	8	50.8	8.9	3			
ap	200.5	7.8	24	198.8	7.8	20	197.3	9.5	17	198.6	7.2	13
–ac	–114.7	18.8	126	–109.1	17.1	129	–106.5	15.9	158	–105.3	14.7	120
–sc	–64.9	12.9	752	–67.7	12.2	847	–67.0	12.2	824	–67.1	12.2	876
α_1	**186.6**	**42.0**	**1 020**	**169.6**	**33.6**	**1 020**	**163.6**	**34.5**	**1 020**	**167.2**	**31.7**	**1 020**
+ac	130.9	14.0	173	133.8	10.3	307	132.2	9.9	416	133.6	10.1	327
ap	180.0	15.5	585	175.6	15.5	600	175.5	16.1	498	175.4	15.6	597
–ac	–122.6	16.9	213	–125.7	17.5	104	–127.5	17.4	98	–128.2	18.2	93
–sc	–77.8	8.1	37	–76.1	6.2	5	–80.4	8.5	3			
Θ_1	**–61.9**	**13.2**	**1 020**	**–57.0**	**18.8**	**1 020**	**–59.4**	**9.8**	**1 020**	**–58.3**	**9.3**	**1 020**
–sc	–62.3	9.9	1 005	–58.1	9.1	1 001	–59.4	9.3	1 015	–58.3	9.0	1 016

TABLE III
(*Continued*)

Angle/ conformational region	HD			HS			ND			NS		
	AV	SD	*N*	AV	SD	*N*	AV	SD	*N*	AV	SD	*N*
b) calculation without cross-energy terms and ε = 4												
α_2	**–76.4**	**31.8**	**1 020**	**–82.8**	**33.6**	**1 020**	**–78.3**	**38.0**	**1 020**	**–79.7**	**31.9**	**1 020**
sp	–4.6	22.9	13	–14.6	11.9	8	0.5	16.3	10	–9.7	22.3	7
+sc	48.7	10.1	10	47.7	7.4	7	50.6	9.7	16	52.9	12.6	11
ap	198.0	8.6	34	200.6	7.3	57	199.2	8.6	56	201.3	6.6	45
–ac	–112.1	19.0	176	–113.8	19.0	241	–112.0	19.0	200	–111.7	18.6	209
–sc	–68.1	12.7	783	–68.6	12.5	703	–68.4	12.6	734	–68.7	12.5	744
α_1	**184.4**	**48.7**	**1 020**	**183.5**	**37.6**	**1 020**	**178.0**	**34.0**	**1 020**	**176.0**	**43.8**	**1 020**
+ac	131.6	12.5	254	132.0	13.6	167	136.3	10.3	220	128.0	18.0	180
ap	177.8	14.7	529	179.6	16.4	636	177.3	15.8	631	180.2	15.3	638
–ac	–116.8	19.5	134	–123.8	16.8	197	–125.5	17.3	163	–128.0	19.5	113
–sc	–76.4	8.9	95	–80.3	8.7	12	–85.3	3.6	3	–76.9	8.3	39
Θ_1	**172.7**	**16.3**	**1 020**	**–58.1**	**17.4**	**1 020**	**–59.6**	**19.9**	**1 020**	**118.3**	**68.9**	**1 020**
+sc	67.3	7.6	6	64.3	4.4	3	67.3	10.9	9	67.9	9.7	605
+ac	141.6	15.3	22							116.1	23.4	13
ap	174.0	9.7	986							173.6	10.0	333
–sc				–59.3	9.8	1 008	–61.5	9.6	1 001	–60.2	11.1	64

TABLE III
(*Continued*)

Angle/ conformational region	HD			HS			ND			NS		
	AV	SD	*N*	AV	SD	*N*	AV	SD	*N*	AV	SD	*N*
c) calculation with cross-energy terms and ε = 1												
α_2	**–73.1**	**22.8**	**1 020**	**–72.7**	**24.3**	**1 020**	**–74.3**	**39.4**	**1 020**	**–61.8**	**29.8**	**1 020**
sp	–16.6	17.2	9	–13.6	15.7	6	11.6	20.4	16	0.2	21.4	36
+*sc*	46.3	5.3	5	52.8	12.2	9	51.7	12.8	44	46.1	10.2	30
ap	202.9	4.5	11	202.7	6.4	15	198.8	7.1	19	201.7	6.4	6
–*ac*	–104.9	14.9	142	–105.8	15.2	123	–109.2	17.0	262	–106.2	15.5	75
–*sc*	–68.1	12.3	849	–68.3	11.9	863	–69.3	13.0	675	–63.6	13.0	869
α_1	**162.2**	**31.6**	**1 020**	**168.7**	**32.4**	**1 020**	**131.0**	**54.1**	**1 020**	**183.1**	**37.7**	**1 020**
+*sc*							76.3	8.7	380	79.7	7.7	26
+*ac*	133.6	9.6	419	135.1	9.6	319	109.9	18.1	200	119.8	19.4	112
ap	174.3	15.4	521	175.3	15.2	600	180.3	14.7	367	183.2	14.6	676
–*ac*	–126.7	16.0	76	–126.2	18.1	91	–132.0	13.1	69	–128.9	14.4	201
Θ_1	**–59.3**	**8.8**	**1 020**	**–57.4**	**9.3**	**1 020**	**59.9**	**19.2**	**1 020**	**56.8**	**20.4**	**1 020**
+*sc*							62.0	9.3	992	59.4	9.1	993
–*sc*	–59.4	8.7	1 018	–57.5	9.1	1 016	–61.5	13.7	16	–60.2	16.0	16

TABLE III
(*Continued*)

Angle/ conformational region	HD			HS			ND			NS		
	AV	SD	*N*	AV	SD	*N*	AV	SD	*N*	AV	SD	*N*
d) calculation with cross-energy terms and ε = 4												
α_2	**–80.9**	**32.3**	**1 020**	**–75.4**	**27.3**	**1 020**	**–78.0**	**27.3**	**1 020**	**–76.1**	**41.6**	**1 020**
sp	–14.1	19.4	4	3.0	18.4	4	–15.1	14.9	11	12.2	20.2	12
+sc	54.8	11.7	11	44.8	8.5	6				49.5	10.7	39
ap	202.1	6.7	42	202.5	7.0	20	201.2	7.2	29	199.5	8.9	46
–ac	–112.6	17.5	239	–111.8	18.0	162	–113.2	17.6	187	–113.6	18.1	233
–sc	–68.7	12.2	720	–67.8	12.0	823	–67.7	13.1	788	–67.6	13.6	686
α_1	**184.7**	**37.0**	**1 020**	**174.7**	**38.6**	**1 020**	**185.1**	**46.9**	**1 020**	**159.1**	**46.4**	**1 020**
+sc							77.4	9.3	11	78.9	8.7	121
+ac	132.5	13.2	171	131.4	12.1	246	131.2	14.7	201	116.0	19.5	214
ap	180.8	15.2	630	176.1	14.6	637	178.9	15.6	588	179.9	15.6	586
–ac	–124.5	18.1	199	–121.4	19.1	93	–118.1	19.8	131	–133.5	13.8	90
–sc	–82.1	5.8	15	–79.4	8.0	38	–77.2	9.9	85	–73.0	9.6	5
Θ_1	**–57.3**	**23.6**	**1 020**	**170.2**	**19.2**	**1 020**	**161.2**	**38.2**	**1 020**	**74.0**	**31.3**	**1 020**
+sc	64.9	14.4	7				66.3	10.5	121	67.1	9.4	955
+ac				144.2	7.8	27	133.9	20.9	25	103.8	19.5	10
ap	172.5	14.5	6	168.9	9.2	974	174.5	10.1	865	175.7	12.4	46
–sc	–59.6	9.5	998	–70.5	15.3	12	–62.0	17.1	4	–57.1	9.4	4

point in the maps reflects the "best", i.e. the lowest-energy orientation of each torsional angle in the molecule. This was achieved by using the random-walk protocol of RAMM for the Θ_1, Θ_3, γ_1, γ_2, β_1, β_3 angles when the α_2, α_1 map was calculated. The equivalent protocol for α_2, Θ_3, γ_1, γ_2, β_1, β_3 was used during the calculation of the α_1,

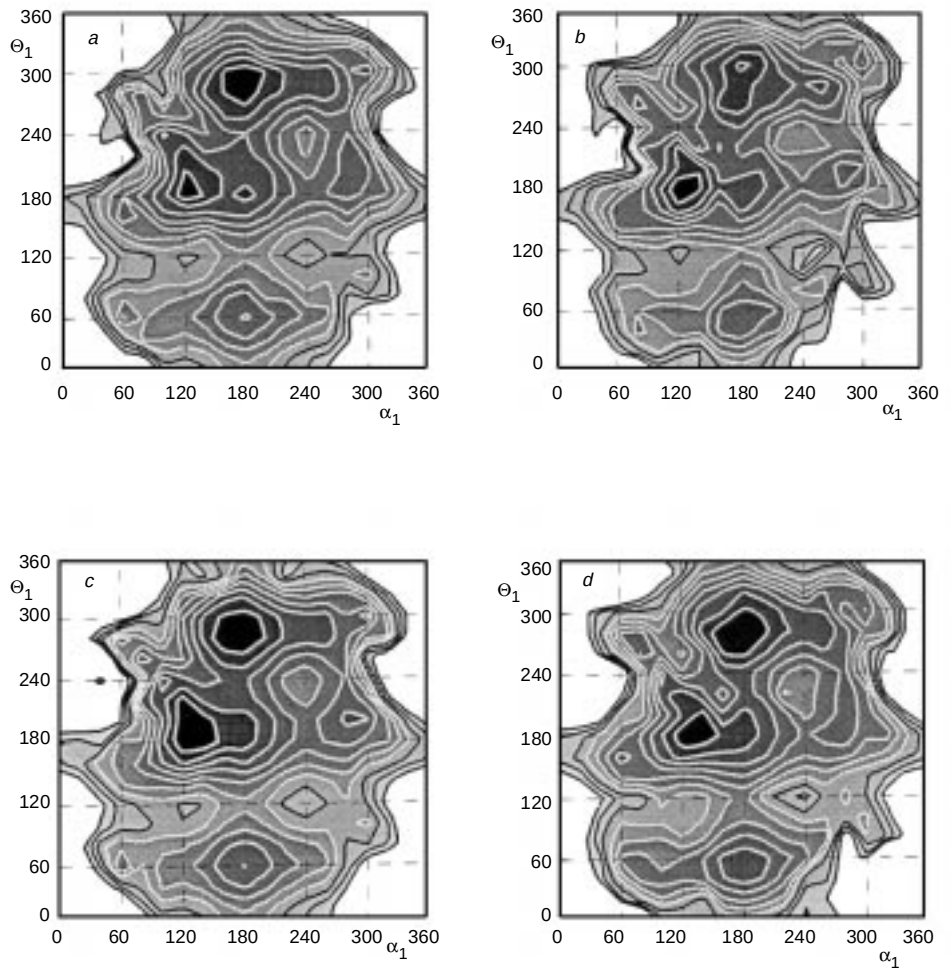

FIG. 8

RAMM α_1/Θ_1 conformational energy maps, calculated by using a dielectric constant of 4. Colour scheme as in Fig. 6. *a* **HD**, *b* **HS**, *c* **ND**, *d* **NS** model molecules

Θ_1 profile. All of the conformations which were indicated as local minima on the two-dimensional surface (bordered within 10 kcal/mol above the global energy minimum of the surface) were selected for further processing, i.e. global energy minimization. The total numbers of final low-energy conformations which were dependent on the conformational energy surface and the selection protocol (see the *rms* description in the METHODS section) of the glycolipid molecule, are summarized in Table IV.

The equilibrium distribution of the conformers as a function of the α_2, α_1 and Θ_1 torsion angle is summarized in Table V. In accordance with the RAMM two-dimensional potential energy surfaces and the results of consecutive geometry optimization (see Table V), two families of conformations are prevalent in the equilibrium mixture:

Conformers with $\alpha_2/\alpha_1/\Theta_1$ = *–sc/ap/–sc* (Fig. 10). This family of conformations is stabilized by the antiparallel orientation of the C1–O1 and N1–H bond dipoles. When a

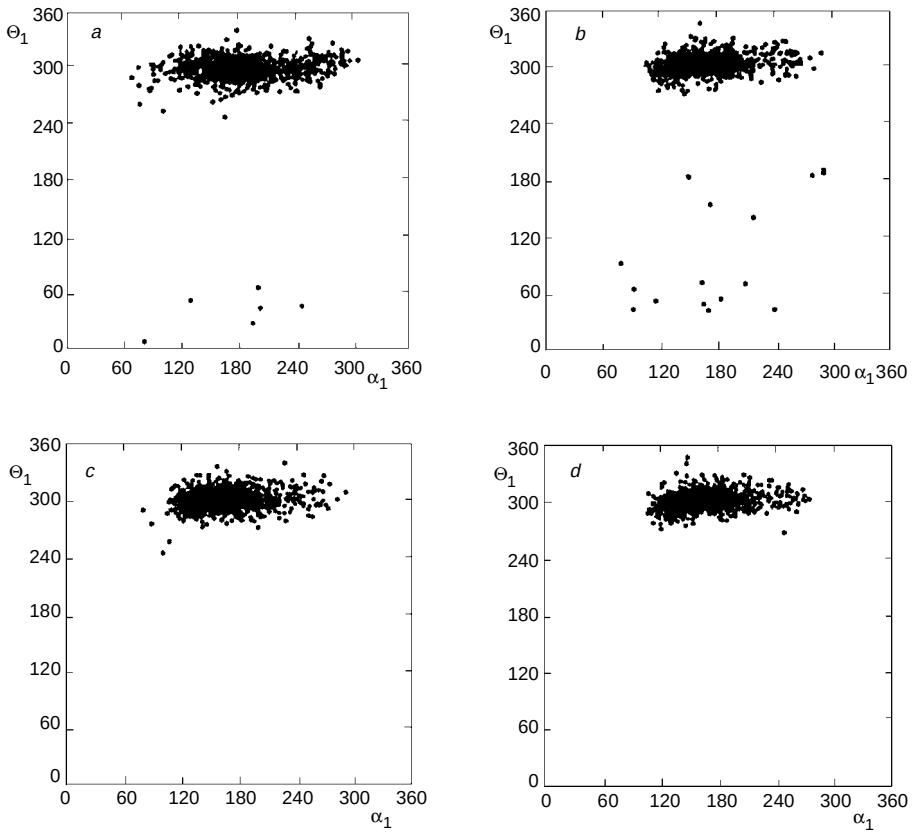

FIG. 9

Scattering of the α_1/Θ_1 torsional angles, as obtained from the 1 020 ps molecular dynamics simulation (asterisks). *a* **HD**, *b* **HS**, *c* **ND**, *d* **NS** model molecules

TABLE IV
Number of low-energy conformers with populations contributing to the equilibrium mixture, obtained from RAMM conformational search calculated with different values of dielectric constants ε

Molecule	ε	
	1.5	4.0
HD	13	21
HS	11	22
ND	12	22
NS	10	14

TABLE V
Number of conformers, *n*, found for the given family characterized by the values of α_2, α_1 and Θ_1 torsional angles, equilibrium population of the conformer family and relative energy of the lowest-energy conformation in the family related to the global energy minimum of the molecule calculated by RAMM with dielectric constants 1.5 and 4. Only those conformations which contribute more than 1% to the equilibrium mixture (calculated at 25 °C) are given. The relative energies are in kcal/mol (1 kcal/mol = 4.1868 kJ/mol)

Molecule	Dihedral angle $\alpha_2/\alpha_1/\Theta_1$	ε = 1.5			α = 4.0		
		n	x_i	Δ*E*	*n*	x_i	Δ*E*
HD	*–sc/+ac/ap*	3	51.7	0.0	2	10.5	0.79
	–sc/ap/–sc	5	46.4	0.34	4	78.8	0.0
	–sc/+ac/–ac				1	6.3	0.97
	+sc/–ac/–sc	3	<1		2	1.7	1.49
	–sc/ap/ap				1	1.1	1.65
HS	*–sc/+ac/ap*	4	95.9	0.0	4	45.8	0.13
	–sc/ap/–sc	3	3.9	1.41	5	49.8	0.0
	–sc/+ac/–sc	1	<1		1	3.2	1.02
ND	*–sc/+ac/ap*	3	49.7	0.0	2	33.6	0.04
	–sc/ap/–sc	3	45.0	0.18	4	63.1	0.0
	+sc/–ac/–sc	3	5.1	0.84	2	1.3	1.34
NS	*–sc/+ac/ap*	4	98.0	0.0	4	39.2	0.38
	–sc/ap/–sc	2	1.8	1.50	3	57.7	0.0
	–sc/+ac/–sc	1	<1		1	2.4	1.23

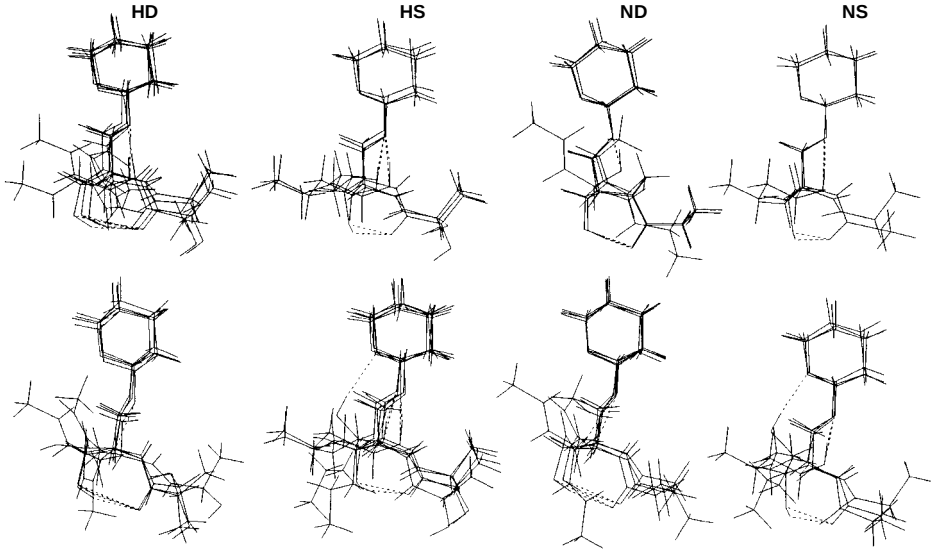

FIG. 10

Superposition of the low-energy conformers with $\alpha_2/\alpha_1/\Theta_1$ = *–sc*/*ap*/*–sc* as obtained from the RAMM conformational search and subsequent geometry optimization. The intramolecular hydrogen bonding is indicated by a broken line. Dielectric constant ε = 1.5 (top) and ε = 4 (bottom)

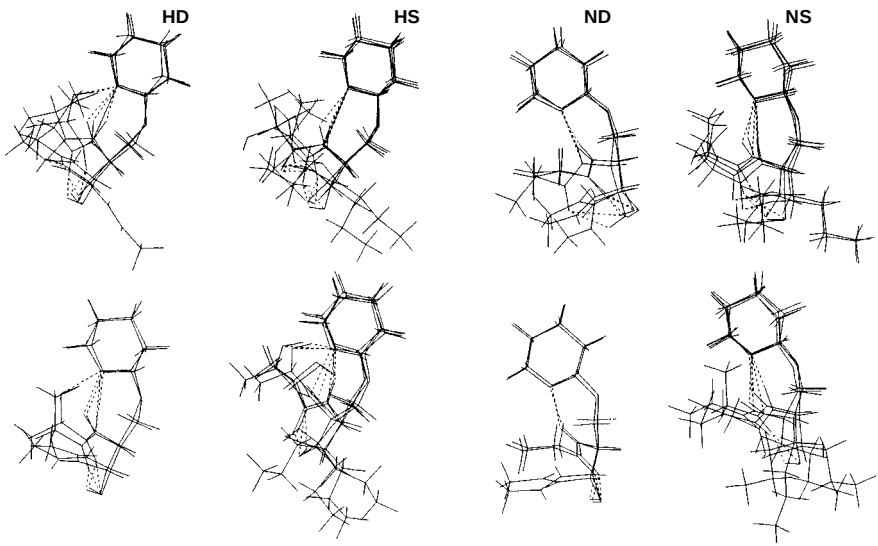

FIG. 11

Superposition of the low-energy conformers corresponding to the $\alpha_2/\alpha_1/\Theta_1$ = *–sc*/*+ac*/*ap* family of conformations. The intramolecular hydrogen bonding is indicated by a broken line. Dielectric constant ε = 1.5 (top) and ε = 4 (bottom)

low dielectric constant value was used during the RAMM conformational search, the equilibrium population of the molecules with C4–C5 single bond (**HS**, **NS**) was considerably reduced. On the other hand, if a double bond between the C4–C5 atoms in the sphingosine chain is present (**HD** and **ND**), this family of conformers is populated almost 50%. The same conformational search with a dielectric constant of 4 provided quite a different prediction of the equilibrium mixture: although the *–sc*/*ap*/*–sc* family remains the main conformation for all types of molecules, the contribution is different: the lowest value of 49.8% was obtained for the **HS** molecule and the highest value 78.8%, for the **HD** molecule. The distributions for **ND** and **NS** are similar, near 60%.

Conformers with $\alpha_2/\alpha_1/\Theta_1$ = *–sc/+ac/ap*. As indicated by broken lines in Fig. 11, many conformers in this family are stabilized by intramolecular hydrogen bonding between the amide hydrogen and the oxygen of the pyranose ring. The population of this family of conformers reaches almost 100% for molecules with a single bond in the sphingosine chain (**HS** and **NS**, see Table V). This distribution is valid for conformational search with a dielectric constant of 1.5. On the other hand, in the case of the molecules with a double bond (**HD** and **ND**), the conformer family contributes 50% to the equilibrium. The results of the conformational search with $\varepsilon = 4$ indicate a still larger decrease in the contribution of this family to the equilibrium: 10.5% for **HD**, 45.8% for **HS**, 33.6% for **ND**, and 39.2% for **NS**.

The structure of the hydrocarbon chains has a minor effect upon the orientation of the sugar-ceramide linkage.

CONCLUSIONS

A similar conformational flexibility for the α_2, α_1 torsional angles is predicted for all the model glycolipid molecules under study, independently of the modelling protocol used, i.e. random molecular mechanics (RAMM) or molecular dynamics (MD). Also, the value of the dielectric constant and other parameters used in the calculation setup (i.e. the use of the cross-energy terms in the energy expression) does not affect appreciably the conformational fluctuation in the direction of those angles.

A different conformational flexibility is predicted for the Θ_1 torsional angle. Based on the population distribution of conformers using the RAMM energies (dielectric constant 1.5) we can assume that the molecules with the single bond in the sphingosine chain strictly prefer the *ap* conformer for the Θ_1 angle. In contrast to this, the prototype molecules containing a double bond in the ceramide part exhibit a conformational equilibrium between the *ap* and *–sc* conformations. Applying a dielectric constant of 4, a conformational equilibrium between the two conformations is also obtained for the **HS** and **NS** molecules with the single bond in the sphingosine chain.

Molecules similar to our **HD** and **ND**, namely GlcCer(h) (i.e. β-D-glucosylceramide with 2-D-hydroxy fatty acid) and GlcCer(n) (i.e. β-D-glucosylceramide containing 4

sphingenine), have been studied recently by Nyholm and Pascher[10,11]. Our prediction for the +*sc* : *ap* : –*sc* population of the rotamers for Θ_1 (calculated at $\varepsilon = 1.5$) is similar to the results for the more complex molecules of GlcCer(h) and GlcCer(n) calculated with $\varepsilon = 4$ and GlcCer(h) calculated with $\varepsilon = 1.5$ (refs[10,11]). This indicates that the presence of hydroxylic groups in glucose may not affect the Θ_1 rotamer populations considerably. On the other hand, when compared, the results obtained with the same dielectric constant are in a poorer agreement. The +*sc* : *ap* : –*sc* ratio of Θ_1 for the two molecules, GlcCer(h) and GlcCer(n), exhibits a similar value at $\varepsilon = 80$ (GlcCer(h)/10 : 56 : 34; GlcCer(n)/11 : 55 : 33) and $\varepsilon = 4$ (GlcCer(h)/4 : 44 : 52; GlcCer(n)/4 : 47 : 48), whereas at $\varepsilon = 1.5$ the ratios differ substantially (GlcCer(h)/0 : 49 : 51, GlcCer(n)/1 : 75 : 23)[10]. Table V demonstrates that our equilibrium results for the four molecules studied are more sensitive to the dielectric constant than the values of Nyholm and Pascher[10]. The differences can be due to the different geometric models – the totally flexible model used in the RAMM calculation while part of the molecule fixed in experimental geometry for GlcCer(h) and GlcCer(n). In addition, the dielectric constant dependent scaling of the bond lengths of the amide group as a part of the original MM2 parametrization can induce some changes in the geometric and energy properties of the molecule, which are more appreciable in the fully relaxed model.

The prediction of the conformational flexibility for the Θ_1 torsional angles has also been shown to be very sensitive to the optional parameters used in the molecular dynamics simulation. In the majority of the different simulations we did not observe all of the three possible conformations, i.e. +*sc*, *ap* and –*sc* of Θ_1, simultaneously. In fact, a single conformational region was predicted for the Θ_1 angle. The dominant conformation differed from molecule to molecule. It seems obvious that the duration of the MDs (1ns) failed to be long enough to sample all the assumed conformational regions. This problem of conformational sampling for the Θ_1 angle could probably be overcome by following the proposal of Sun and Kollman[34], i.e. by increasing the simulation temperature. Sun and Kollman suppose that increase in the simulation temperature contributes to the efficiency of the conformational space sampling more than the expansion of the simulation time scale. Moreover, the influence of the force field parametrization as one of the possible sources of diversity of the results of the conformational flexibility for the Θ_1 torsional angle, as obtained from the molecular dynamics simulations, should be further investigated.

Finally, taking into account the complexity of the real biological membranes, the inter- and intramolecular interactions between the large molecular assemblies composed of lipids, proteins, ions and solvent molecules should be modelled and analyzed. The "quality" of the parametrization of the force field method is equally important for such comprehensive studies of membrane fragments. From this point of view, the testing and comparison of the ability of the available computational methods to properly

predict molecular conformations is a very important preparatory step for state-of-the-art computer modelling of the dynamics of real membrane fragments.

This work was supported by Grant No. 1354 from the Slovak Grant Agency. Z. G. is grateful to the Deutscher Akademischer Austauschdienst (DAAD) for travelling grant, allowing her to visit Dr C.-W. von der Lieth, Deutsches Krebsforschungszentrum, Heidelberg, Germany, where also the molecular dynamics simulations were calculated and processed. The authors also wish to thank Dr C.-W. von der Lieth for valuable discussions and careful reading of the manuscript. T. K. acknowledges the Max Planck Institute for Medical Research, Heidelberg, for the opportunity to use the computer facilities (hardware and MPI licensed software) for data analysis and interactive graphics.

REFERENCES

1. Curatolo W.: Biochim. Biophys. Acta *906*, 111 (1987).
2. Curatolo W.: Biochim. Biophys. Acta *906*, 137 (1987).
3. Karlsson K. A.: Annu. Rev. Biochem. *58*, 309 (1989).
4. Nyholm P. G., Pascher I., Sundell S.: Chem. Phys. Lipids *52*, 1 (1990).
5. Karlsson K.-A. in: *Biological Membranes* (D. Chapman, Ed.), Vol. 4, p. 1. Academic Press, London 1982.
6. Abrahamsson S., Dahlen B., Pascher I.: Acta Crystallogr., B *33*, 2008 (1977).
7. Pascher I., Sundell S.: Chem. Phys. Lipids *20*, 175 (1977).
8. Skarjune R., Oldfield E.: Biochemistry *21*, 3154 (1982).
9. Wynn C. H., Marsden A., Robson B.: J. Theor. Biol. *119*, 81 (1986).
10. Nyholm P.-G., Pascher I.: Biochemistry *32*, 1225 (1993).
11. Nyholm P.-G., Pascher I.: Int. J. Biol. Macromol. *15*, 43 (1993).
12. Allinger N. L., Kok R. A., Imam M. R.: J. Comput. Chem. *9*, 591 (1988).
13. Allinger N. L., Yuh Y. H., Lii J.-H.: J. Am. Chem. Soc. *111*, 8551 (1989).
14. von der Lieth C.-W., Kozar T., Hull W. E.: Unpublished results.
15. Bassolino-Klimas D., Alper H. E., Stouch T. R.: Biochemistry *32*, 12624 (1993).
16. De Loof H., Harvey S. C., Segrest J. P., Pastor R. W.: Biochemistry *30*, 2099 (1991).
17. Huang P., Perez J. J., Loew G. H.: J. Biomol. Struct. Dyn. *11*, 927 (1994).
18. Stouch T. R.: Mol. Simul. *10*, 335 (1993).
19. Stouch T. R., Ward K. B., Altieri A., Hagler A. T.: J. Comput. Chem. *12*, 1033 (1991).
20. Venable R. M., Zhang Y., Hardy B. J., Pastor R. W.: Science *262*, 223 (1993).
21. Kozar T., Petrak F., Galova Z., Tvaroska I.: Carbohydr. Res. *204*, 27 (1990).
22. French A. D., Dowd M. K.: J. Mol. Struct. (Theochem) *286*, 183 (1993).
23. Tocanne J. F., Teissie J.: Biochim. Biophys. Acta *1031*, 111 (1990).
24. Ermer O., Lifson S.: J. Am. Chem. Soc. *95*, 4121 (1973).
25. Hagler A. T., Osguthorpe D. J., Dauber-Osguthorpe P. D., Hempel J. C.: Science *227*, 1309 (1985).
26. Hagler A. T. in: *The Peptides* (J. Meienhofer, Ed.), Vol. 7, p. 213. Academic Press, New York 1985.
27. Sundaralingam M.: Ann. N. Y. Acad. Sci. *195*, 324 (1972).
28. Gibson K. D., Scheraga H. A. in: *Structure* (R. Sharma and M. H. Sharma, Eds), Vol. 1, *From Proteins to Ribosomes*, p. 67. Academic Press, New York 1988.
29. Li Z., Scheraga A.: Proc. Natl. Acad. Sci. U.S.A. *84*, 6611 (1987).

30. Abrahamsson S., Pascher I.: Acta Crystallogr. *21*, 79 (1966).
31. Hauser H., Pascher I., Sundell S.: J. Mol. Biol. *137*, 249 (1980).
32. Elder M., Hitchcock P., Mason R., Shipley G. G.: Proc. R. Soc. London, A *354*, 157 (1977).
33. Pearson R. H., Pascher I.: Nature *281*, 499 (1979).
34. Sun Y., Kollman P. A.: J. Comput. Chem. *13*, 33 (1992).